Int. J. Electrochem. Sci., 14 **(2019)** 9436 – 9448, doi: 10.20964/2019.10.34

International Journal of ELECTROCHEMICAL SCIENCE
www.electrochemsci.org

The Synthesis of Bridging Carbon Particles with Carbon Nanotubes from *Areca catechu* Husk Waste as Supercapacitor Electrodes

E. Taer[1,], R. Handayani[1], Apriwandi[1], R.Taslim[2], Awitdrus[1], A. Amri[3], Agustino[1] and I. Iwantono[1]*

[1] Department of Physics, University of Riau, 28293 Simpang Baru, Riau, Indonesia
[2] Departement of Industrial Engineering, State Islamic University of Sultan Syarif Kasim, 28293 Simpang Baru, Riau, Indonesia
[3] Department of Chemical Engineering, University of Riau, 28293 Simpang Baru, Riau, Indonesia
[*]E-mail: erman_taer@yahoo.com

Received: 4 June 2019 / *Accepted:* 28 July 2019 / *Published:* 30 August 2019

This study examines the synthesis of carbon particles with nanotubes as electrodes for supercapacitors. The electrodes were made from areca catechu husk without the addition of adhesive materials. There was a multi-activation process including chemical and physical activation using KOH activator and CO_2. Physical activation time is the main factor for consideration in this discussion. The addition of activation time has an effect on the physical and electrochemical properties of supercapacitor electrodes. Carbon hollow fiber is clearly visible on the surface of the electrode with varying sizes of outer and inner diameters in the nanometer range. The results show there was an incredible performance by ACF-2.5 sample activated for 2.5 hours. ACF-2.5 sample delivered optimum capacitive properties of 165 F g^{-1} with a maximum surface area of 757.449 m^2 g^{-1}. Thermogravimetric analysis and the degree of crystallinity were also carried out to strengthen the electrode analysis of supercapacitors.

Keyword: carbon fiber; areca catechu husk; supercapacitor

1. INTRODUCTION

Nanomaterials are a type of smart material widely used in various fields, including solar cells, batteries, and supercapacitors [1]. The nanostructured materials such as nanotubes, nanofibers, nanobelts, and nanowires are widely studied today [2]. Of all these, nanofibers have the advantage of a homogeneous pore structure consisting of mesopores and micropores. Nanocellulose is an alternative raw material in the production of the nanofiber. Moreover, it is a major component in the structure of plant cell walls [3] and might be converted into carbon nanofibers through the carbonization process.

Carbon nanotubes are widely used as supercapacitor electrodes since they are advantageous in ion diffusion processes, especially the inner surface of nanotube, compared to nanofiber structures. Additionally, the hollow structure of the nanotubes increases the surface area of the carbon electrodes which are significantly proportional to the increase in capacitive properties. Areca catechu husk is an example of a biomass material with a fine fiber structure ranging from 60% to 80% of the total weight of fresh fruit [4]. This is a waste containing hemicellulose (35-64.8%), lignin (13-26%), pectin and pro-pectin [5]. Its production in Indonesia was 47.10 tons based on 2015 data and was expected to increase in subsequent years [6]. In general, it is used as a cosmetic and slimming ingredient, medicinal raw materials, antidepressants, and cigarette substitutes [7]. The abundant production leads to a lot of husks with high content of nano-cellulose, making it a basic material in the preparation of carbon nanofiber.

Nanofibers with hollow structures are among the nano-cellulose contained in the husk. The Carbon nano-cellulose fiber is obtained by activating and carbonizing biomass materials. The activation is conducted in two ways, chemical, and physical processes. In this study chemical activation, therefore, involved the use of KOH as a pore-forming agent increasing specific surface area of the material [8]. Physical activation using CO_2 gas at 900 ˚C with a variation of 1.5 hours, 2 hours, 2.5 hours and 3 hours aimed to break the carbon chain, opening the pores and increasing the carbon surface area. The carbonization process is carried out through combustion using nitrogen gas at a temperature of 600 ˚C. This study examined the nanotube structures on carbon electrodes based on areca catechu fibers. The diameter of the nanotube cavity was 40 nm while the highest capacitance obtained was 165 F g^{-1}.

2. EXPERIMENTAL SECTION

Areca catechu husk was collected and pounded to obtain finer fibers. The samples were sun-dried for two days before using an oven with a temperature of 110 ˚C for 2x24 hours. The dried sample was pre-carbonized at a temperature of 250 ˚C for 2.5 hours. It was then crushed with mortar and ground using a ball milling machine for 20 hours to obtain a powder sample with a particle size of 53 µm. The powder was chemically activated using a 0.5 M KOH. It was then transformed into a pellet-shape with a mold diameter of 2 cm at a pressure of 8 tons. The pellet-shaped samples were carbonized and physically activated. Furthermore, the carbonization process begins at room temperature and rises to 600 ˚C in the N_2 gas atmosphere, followed by physical activation at 900 ˚C using CO_2 [9, 10]. Based on variation of activation time, all samples labeled ACF-1.5, ACF-2.0, ACF-2.5, and ACF-3.0 which mean, AC is activated carbon and the number are variation of activation time. The chosen variation of activation time is 1.5, 2.0, 2.5, and 3.0 hours and the physical and electrochemical properties of the samples were characterized based on density, surface morphology using scanning electron microscopy (SEM) and the chemical content through energy dispersive X-Ray (EDX) method. Additionally, the crystallization structure was analyzed using XRD method and the specific surface area elucidate using BET method. Characterization of electrochemical properties was carried out to determine specific capacitance using the cyclic voltammetry (CV) method with a potential range of 0-500 mV and a scan

rate of 1 mV s^{-1} in the 1 M H_2SO_4 electrolyte solution. The specific capacitance is calculated using the standard equation [11, 12].

3. RESULTS AND DISCUSSION

3.1. Density Analysis

The changes in the density of carbon electrodes after carbonization-physical activation are presented in Table 1. Chemical activation using KOH activators reduces the sizes of the carbon particles, leading to dominant micro pore formation [13]. The physical activation using CO_2, therefore, aimed to produce a strong carbon pellet with larger pores to obtain the best size variation. The impurities in carbon electrodes furthermore are reduced, leading to a reduction in density as a result of opening carbon pores. The Physical activation period greatly affects the value of the density produced. The longer variations in time cause evaporation of materials other than carbon, leading to more mass decreases. This results in higher density shrinkage in the sample carbon pellets. Disposal of impurities causes the opening of more pore structures, leading to greater electrode porosity. Consequently, the greater the porosity lessens the density. Moreover, physical activation causes evaporation of materials other than carbon and finally produce the new formation of pores in the sample electrodes. In general, pore formation is followed by a reduction in mass and the density of the electrodes.

The highest change in carbon density before and after the carbonization-physical activation process was in the ACF-2.5 sample with large density shrinkage of 0.39406 g cm^{-3}, followed by ACF-2.0, ACF-3.0, and ACF-1.5 with shrinkage densities of 0.35784 g cm^{-3}, 0.34146 g cm^{-3}, and 0.24782 g cm^{-3}, respectively. Figure 1 in the ACF-1.5 to ACF-2.5 sample shows the density shrinkage value is in accordance with the theory, but in the ACF-3.0 sample, the shrinkage value is lower than ACF-2.0 and ACF-2.5. This is due to the fact that the ACF-2.5 sample has reached optimum physical activation time. This data trend is in line with another study discussing the effect of activation time on electrodes made from biomass material such as sago waste [14].

Table 1. Density data for all samples

Sample codes	Before pyrolisis	After pyrolisis
ACF-1.5	1.105	0.857
ACF-2.0	1.126	0.768
ACF-2.5	1.094	0.701
ACF-3.0	1.097	0.755

3.2. Thermogravimetric analysis

The Thermogravimetric analysis (TGA) method is used to determine changes in sample mass caused by temperature variations using pyrolysis gas with a maximum temperature of 600 ˚C. The differences in mass are caused by changes in the physical and chemical properties of materials. The Differential Thermal Gravimetry (DTG) data shows the rate of change in sample mass against an

increase in temperature. Furthermore, the change in mass is expressed in percentage. Figure 1 show the TG and DTG curves resulting from the characterization carried out at the Integrated Biomass Laboratory of Lampung University.

The line and black line are the TG and DTG data in time function. The TG curve shows a downward trend indicating a mass shrinkage. Significant mass losses occur at temperature ranges of 0 ˚C to 203 ˚C, probably 8.56%, indicated by the curvature of the TG curve. The first decrease occurs due to the decomposition of the water content contained in the sample. The second mass shrinkage is the largest decrease in the TG which occurred at temperatures range of 203 ˚C to 350.2 ˚C, around 43.82% drop. Depreciation occurs due to the decomposition of complex compounds of sample materials such as hemicellulose, cellulose, and lignin. Furthermore, the lignin mass reduction still continued at a temperature range of 0-550.4 ˚C, where a 61.73% mass shrinkage occurred. The DTG curve shows the maximum mass reduction in a time function experienced by the sample is 0.211 mg min^{-1} occurring at a temperature of 305.5 ˚C as indicated by the peak on the curve. This point shows the fastest shrinkage of mass with a decrease in complex compounds occurring simultaneously. The analysis of thermogravimetric properties is nearly the same as the research outcome of carbon electrodes made from other biomass such as coffee waste [15] and coconut shell [16].

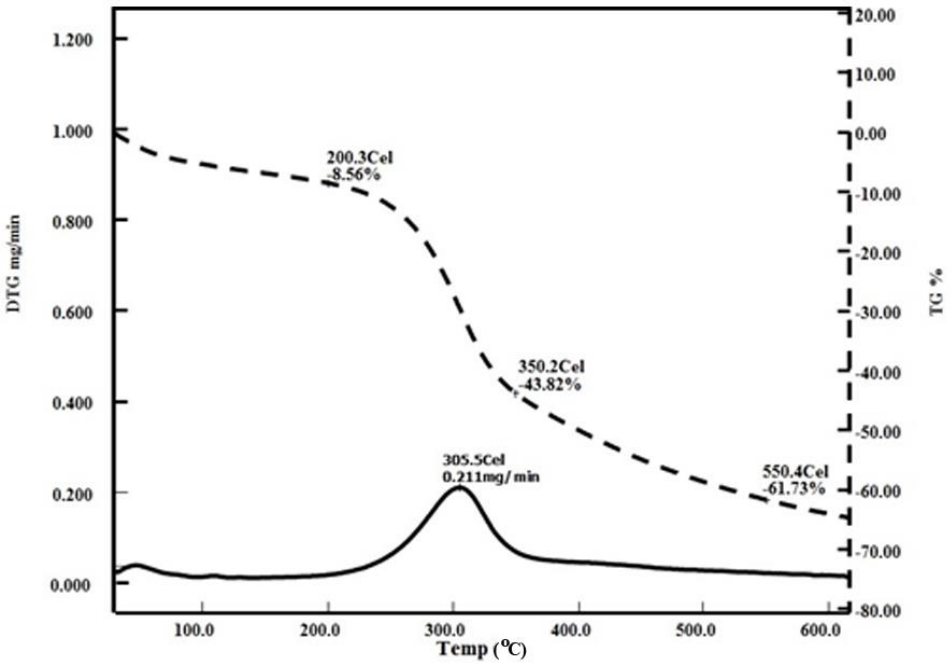

Figure 1. TG and DTG profile for pre-carbonized powder sample

3.3. Surface morphological analysis

The characteristics of the surface morphological structure of carbon electrodes made from areca catechu husk were determined using the Scanning Electron Microscopy method. SEM data for all samples with a magnification of 5000x and 40000x are shown in Figure 2. Basically, the SEM micrograph of 5000x magnification show surface morphology of the samples consisting of carbon

material in particles and fibers at a micrometer scale. The carbon fiber is derived from areca catechu husk consisting of cellulose fiber. Additionally, the SEM micrograph data with 40000X magnification is focused on observing the size and shape of carbon fiber on the variation of physical activation time. The fiber turns often have the shape of a hollow rod and this structure resembles a carbon nanotube (CNT). The SEM micrograph data at 5000x magnification is shown in figure 2.a, 2.b, 2.c, and 2.d for ACF-1.5, ACF-2.0, ACF-2.5 and ACF-3.0 samples respectively. Figure 2.a shows the surface morphology of a sample consisting of many carbon fibers attached to the surface of the particle. The particle size has a range between 1707 nm - 5021 nm and fiber length spread evenly on the surface of carbon particle in the range of 2300 nm - 5210 nm. Figure 2.b presents more of the fine and short carbon fibers spreading and covering the walls of the particles. The particle size is not much different from image 2.a, probably 900 nm - 3554 nm. the length of carbon fiber varies in the range of 200 nm 1000 nm. This size is much smaller than the carbon fiber sample in the ACF-1.5 due to the addition of physical activation time which causes the carbon fiber to shrink and shorten the fiber length. Figure 2.c shows the surface morphology in the ACF-2.5 sample with various carbon fiber lengths. The ACF-2.5 sample has the smallest particle size with a range of 698 nm - 3313 nm, and probably has better pore properties than the ACF-1.5 and ACF-2.0 samples. The carbon fiber length ranges from 1034 nm - 4852 nm. The surface morphology of the ACF-2.5 sample compared to ACF-1.5 and ACF-2.0 samples are clearly different in terms of particle and fiber size. Additionally, the particles appear smaller in size while the fiber is not very dominant compared to samples of ACF-1.5 and ACF-2.0. Figure 2.d shows the surface morphology of the ACF-3.0 sample which has agglomerate and wavy carbon fiber covering almost all the observed areas. The fiber is longer and bigger compared to other samples.

Figure 2.e, 2.f, 2.g, and 2.h are SEM data at 40000X magnification for samples of ACF-1.5, ACF-2.0, ACF-2.5 and ACF-3.0 respectively. The fiber structure with inner diameter sizes ranging from 71 nm - 118 nm and outer diameter 105 nm - 118 nm in 2.e. Figure 2.f are hollow carbon and similar to the ACF-1.5 sample in Figure 2.e, though with a smaller diameter size. The inner diameter sizes in the sample ranged from 56 nm - 74 nm and 85 nm - 126 nm in the outer. Figure 2.g shows an uneven carbon fiber structure and a smaller diameter size for ACF-2.5 sample. The inner diameter size in this sample ranges from 40 nm - 80 nm and 70 nm - 122 diameter for outer. Changes in the size of the diameter and structure of carbon fiber are influenced by the addition of physical activation time which increases the shrinkage and changes the structure to uneven. In figure 3.h carbon fiber for the ACF-3.0 sample are very large with inner and outer diameters ranging from 165 nm - 228 nm and 193 nm - 275 nm respectively. Carbon fiber walls are dominated by holes, giving the fiber uneven look. This is due to the fact that the activation time is too long. In general, the fiber sizes in this study is smaller compared to some previous works on carbon fiber as a supercapacitor electrode such as the ones made from banana stem [17], *Terminalia catappa* leaf [18] and pineapple crown [19].

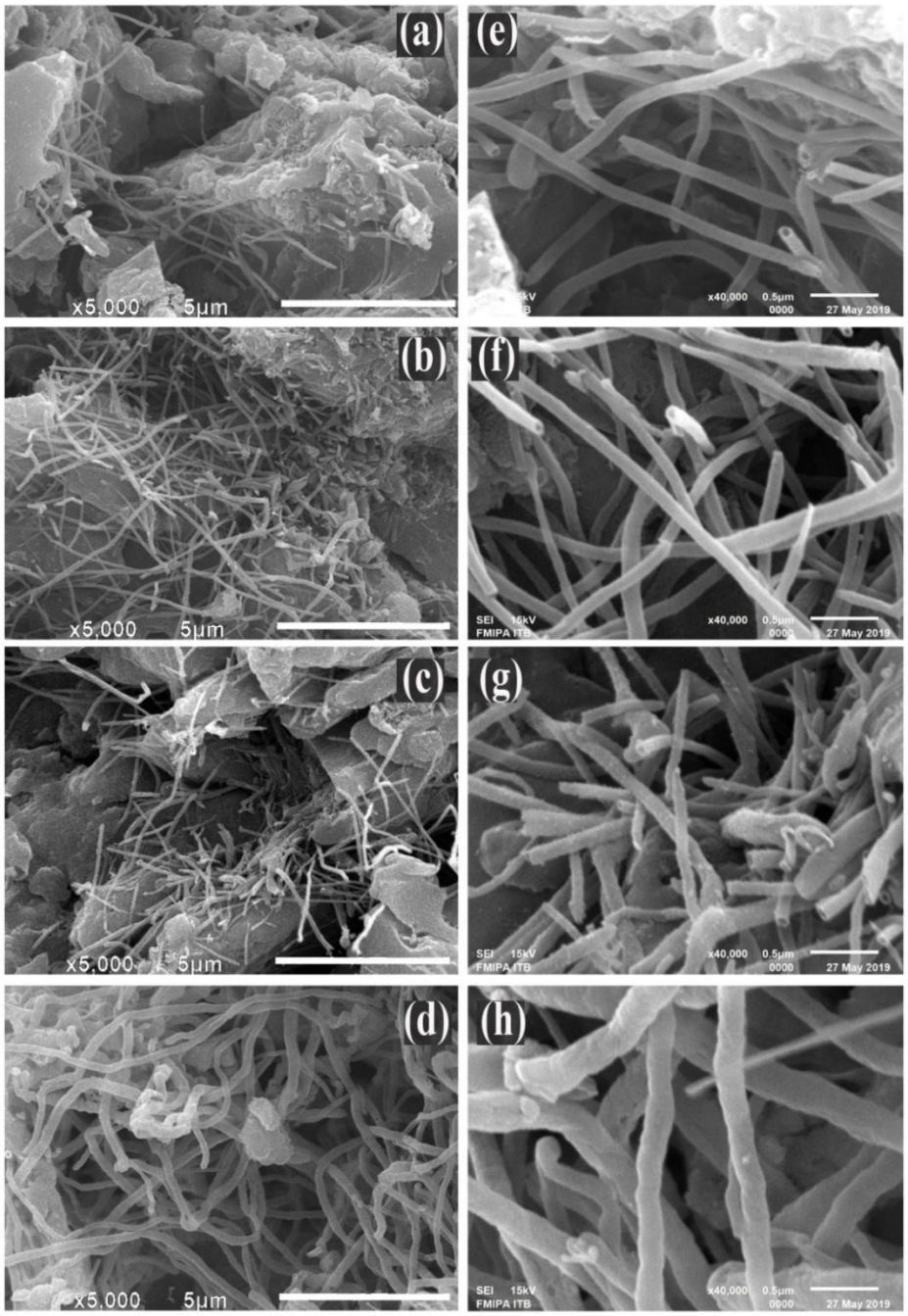

Figure 2. The SEM image with 5000x of magnification for a) ACF-1.5; b) ACF-2.0; c) ACF-2.5; d) ACF-3.0 and The SEM image with 40000x of magnification for e ACF-1.5; f) ACF-2.0; g) ACF-2.5;h) ACF-3.0

3.4. Element content analysis

Energy Dispersive X-Ray Analysis (EDX) is meant to determine the element contents in the carbon electrode. The EDX analysis shows the purity level of carbon and other elements as shown in Table 2. The element contents are grouped in percentages by weight and atomic size. Based on the highest percentage, the elements are Carbon (C), Oxygen (O), Silica (Si), Potassium (K), Magnesium

(Mg), Calcium (Ca) and Sodium (Na). The composition is dominated by carbon at 81% - 92%. These indicate the synthesized sample contains the needed pure carbon. This carbon content is almost the same as those ones from the studies on bamboo waste [20] and jackfruit peel [21]. Besides, oxygen is the other dominant element other than carbon and might be obtained from the CO_2 activation, while the presence of silica elements is attributed to biomass raw material [18]. Potassium elements are also found in many samples due to the use of KOH activators and the washing of samples of carbon electrodes is less neutral [14,18].

Table 2. The element contents for ACF-1.5, ACF-2.0, ACF-2.5 and ACF-3.0 samples.

Elements	Sample codes							
	ACF-1.5		ACF-2.0		ACF-2.5		ACF-3.0	
	Weight (%)	Atom (%)	Weight (%)	Atom (%)	Weight (%)	Atom (%)	Weight (%)	Atom (%)
Carbon	72.67	81.41	86.75	91.04	87.02	91.22	88.46	92.10
Oxygen	17.43	14.66	9.29	7.32	9.19	7.23	8.68	6.78
Silica	3.32	1.59	2.37	1.06	2.59	1.16	1.61	0.72
Pottasium	3.62	1.25	1.33	0.43	1.20	0.39	1.25	0.40
Magnesium	0.45	0.25	-	-	-	-	-	-
Calsium	2.50	0.84	-	-	-	-	-	-
Sodium	-	-	0.26	0.15	-	-	-	-
Totals	100%							

The EDX analysis results in Table 2 show the least carbon quantity is in the ACF-1.5 sample, around 81.41%, followed by ACF-2.0, ACF-2.5 and ACF-1.5 with 91.04%, 91.22% and 92.10% respectively. From this data, longer activation time produced higher carbon. The oxygen content also decreases with an increase in the activation time. This is due to the fact that oxygen decomposes during the activation process. The EDX analysis shows the ACF-3.0 sample has the highest carbon element even though it does not contain the highest capacitance. The highest specific capacitance was in the ACF-2.5 sample.

3.5. X-ray diffraction analysis

The X-ray diffraction patterns at 2θ angles scattering between 10° to 60 ° for carbon electrodes made from acacia catechu husk are shown in Figure 3. Evidently, there are two types of peaks, broad and sharp, in all electrode samples. The broad peak at the 2θ angle at 23° and 44° represents the amorphous structure for carbon material [22], while a sharp peak is a crystal structure. Besides, the ACF-2.0 samples show X-ray diffraction patterns have only one broad peak but many sharp peaks, indicating the electrode surface was characterized by the crystal structure.

The 2θ diffraction angle indicating 002 and 100 planes from all samples are ACF-1.5 is 22,352° and 44,082°, ACF-2.0 sample 42.527°, ACF-2.5 23.111°, and 42.484° and the ACF-3.0 23.924° and 43.680° respectively. The results of X-ray diffraction characterization obtained from the fitting process using Microcal Origin software is shown in Table 3.Table 3 shows lattice parameter

data of carbon electrodes from areca catechu husk. The lattice parameters analyzed were interlayers spacing (d_{002}, d_{100}) and microcrystalline dimensions (L_c and L_a). The d_{002} interlayer spacing changes slightly with increasing activation time on carbon electrodes. It can be concluded that the d_{002} interlayer spacing is inversely proportional to the activation time. The interlayer spacing d_{100} shows irregularity in the addition of physical activation time. From Table 3, the lowest microcrystalline dimension (L_c) is 14.515 Å in the ACF-2.5 sample and the highest L_c, 38.178 Å, in the ACF-1.5. The relationship between microcrystalline dimension (L_c) and specific surface area is expressed by the empirical formula $SSA = 2/\rho L_c$ [23]. Based on this formula, the highest specific surface area is in the ACF-2.5 sample while the lowest is in ACF-1.5 sample. This analysis is supported by the BET surface area measurement data which is fully discussed in the proceeding section.

Table 3. Lattice parameter data of carbon electrodes from areca catechu husk

Sample Codes	$2\theta_{002}$	$2\theta_{100}$	d_{002} (Å)	d_{100} (Å)	L_a (Å)	L_c (Å)
ACF-1.5	22.352	44.082	3.974	2.053	26.489	38.178
ACF-2.0	-	42.527	-	2.124	13.699	-
ACF-2.5	23.111	42.484	3.845	2.126	7.111	14.515
ACF-3.0	23.924	43.680	3.717	2.071	24.865	26.669

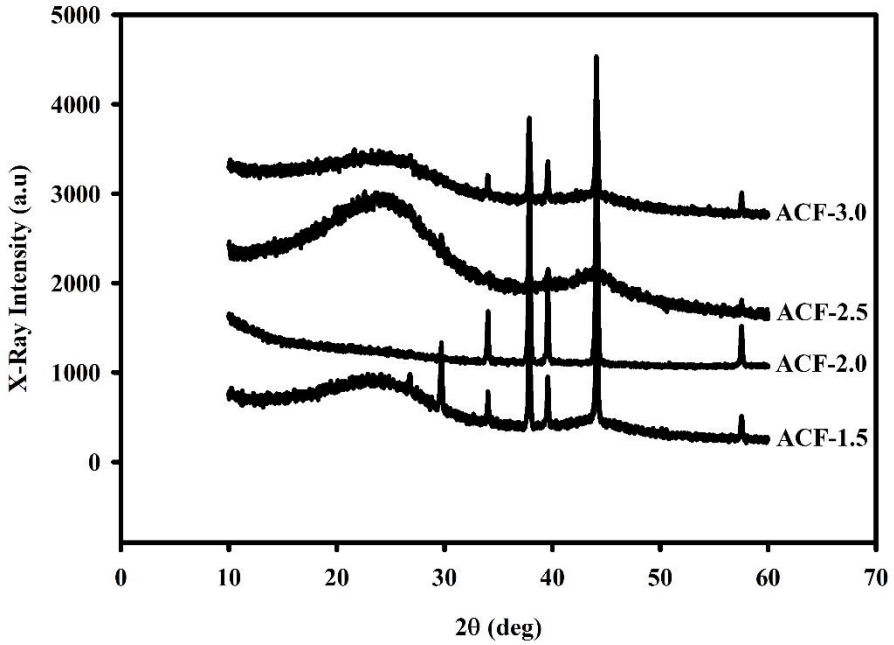

Figure 3. X-ray diffraction pattern ACF-1.5, ACF-2.0, ACF-2.5 and ACF-3.0 samples

3.6. Nitrogen absorption analysis

Nitrogen (N_2) gas absorption test is meant to determine the specific surface area, pore volume and pore size distribution analyzed using the Brunauer Emmet Teller (BET), and the Barrer-Joyner-Halenda (BJH) methods. Figure 4 shows the adsorption curve at a relative pressure of 0 to 1 followed

by desorption process until the pressure becomes 0 again. Based on the pore classification formulated by IUPAC, ACF-1.5, ACF-2.0, ACF-2.5 and ACF-3.0 samples are categorized in IV type with a combination of micro-mesopores [24]. All samples have pore diameters greater than 2 nm as shown in Table 4. Type IV is characterized by a hysteresis loop exhibit at a relative pressure of 0.4. Hysteresis loop refers to widening the micro-pore into mesopores through increases in relative pressure. Pore surface area and pore structure parameters are shown in Table 4. The highest specific surface area is presented by the ACF-2.5 sample, followed by ACF-2.0, ACF-1.5 and ACF-3.0, with 757.449 m^2 g^{-1}, 536.150 m^2 g^{-1}, 492.119 m^2 g^{-1}, and 482.749 m^2g^{-1} respectively. Based on extensive data, the ACF-2.5 sample is likely to produce the highest capacitance the minimum might be at the ACF-1.5 and ACF-3.0 samples due to the lowest surface area data.

Table 4. Physical pore properties of carbon electrode made from areca catechu husk

Sample codes	S_{BET} (m^2g^{-1})	S_{BJH} (m^2g^{-1})	V_{BJH} (cm^3g^{-1})	D_{BJH} (nm)	$D_{average}$ (nm)
ACF-1.5	492.119	24.953	0.0411	3,.14	2.334
ACF-2.0	536.150	23.139	0.0367	3.232	2.291
ACF-2.5	757.449	24.131	0.0353	3.218	2.178
ACF-3.0	482.749	22.817	0.0350	3.204	2.301

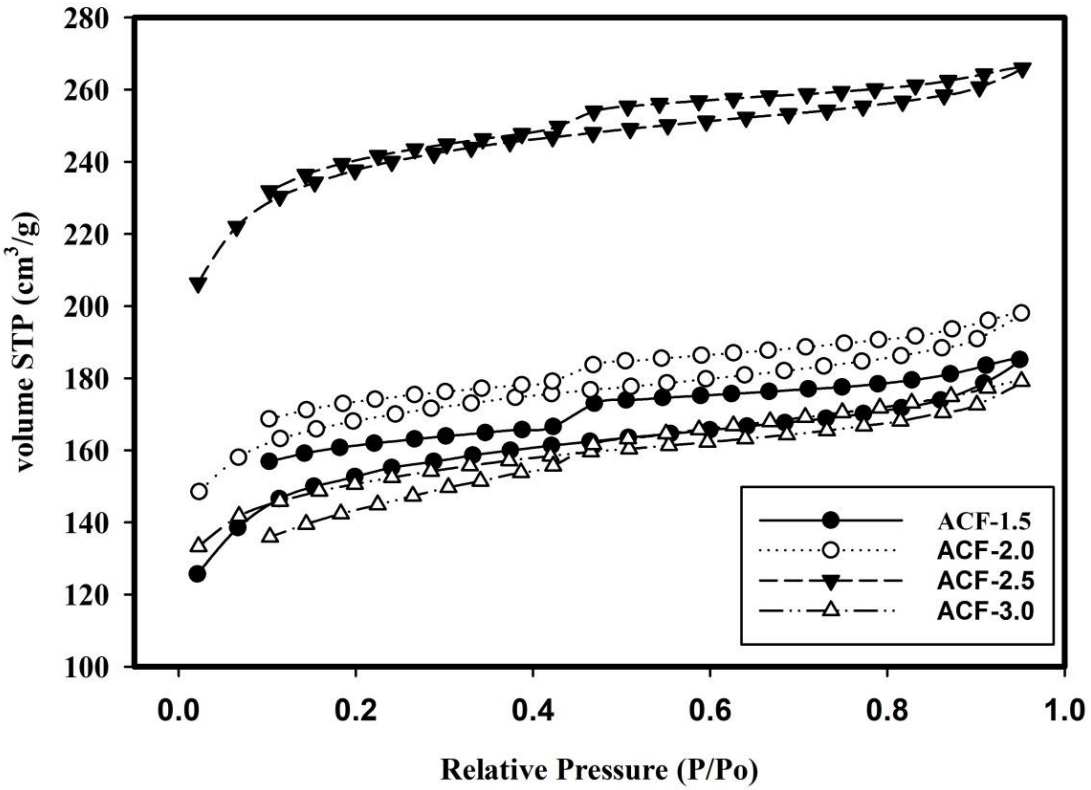

Figure 4. Nitrogen adsorption-desorption isotherms

The BET surface area is very reasonable compared to other biomass resources as shown in Table 6. S_{BJH} and V_{BJH} decreased with an increase in the physical activation time. Nevertheless, the ACF-2.5 sample had an increase in BJH surface area. Specific surface area (S_{BET}) increased rapidly

due to the addition of activation time. The optimum specific surface area was found in samples activated for 2.5 hours. At 3 hours, the specific surface area sample decreased because the addition of activation time makes the pore size wider or even cause damages. Figure 5 shows the relationship between the pore radius volume adsorption of carbon electrodes in the ACF-1.5, ACF-2.0, ACF-2.5 and ACF-3.0 samples. The highest pore volume adsorption is in the ACF-1.5 and ACF-3.0 samples with the pore radius of 1.79 nm. The pore size dominating the sample is the mesopore with the highest absorption volume at a diameter of 3.58 nm. The range of pore radius 2-4 nm indicates a significant change in pore volume. Furthermore, the pore distribution curve tends to flatten or there is no change in pore volume in the radius greater than 5 nm. Information about the trend of changes in absorption rate to the radius is in Figure 5.

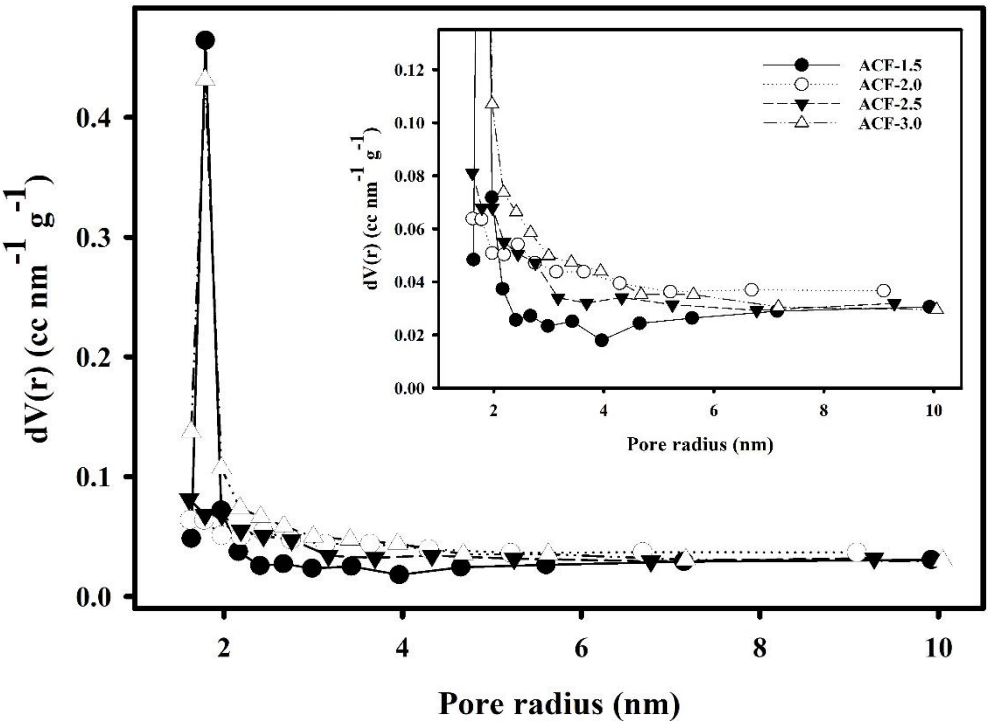

Figure 5. Pore size distribution curves for all samples

3.7. Electrochemical properties analysis

The electrochemical properties of supercapacitor cells were analyzed using the Cyclic Voltammetry (CV) method at a low scanning rate (1 mV s^{-1}). This was meant to facilitate ions perfect diffusion process into the pores of the carbon electrode. Generally, low scanning rates are assumed to produce relatively large capacitances. The CV curve shows the relationship between voltage and current density. The current data is displayed as a charge (I_c) and discharge current (I_d). Moreover, the charge current caused by ions diffusion process enters the electrode pores at a potential of 0 - 0.5 V while the discharge current occurs as the ions leave the pores electrode at a voltage of 0.5 - 0 V, shown in Figure 6. The I-V area in all samples was rectangular shaped, usually the normal type for carbon electrodes made from biomass material [25]. The difference in the rectangular area formed by the charge and discharge currents in the samples is shown in Figure 6. The ACF-2.5 sample has the largest

I-V area, followed by ACF-2.0, ACF-3.0, and ACF 1.5 respectively. For this reason, ACF-2.5 sample is likely to produce the highest capacitance. Basically, Specific capacitance is determined by the standard equation. The (I_c) and (I_d) data, the average mass of electrode (m), and specific capacitance of supercapacitors (C_{sp}) are presented in Table 5. The specific capacitance of the samples of ACF-1.5, ACF-2.0, ACF-2.5 and ACF-3.0 are 100 F g^{-1}, 144 F g^{-1}, 165 F g^{-1} and 126 F g^{-1} respectively. From the results, longer activation time increase the specific capacitance. The optimum capacitance found in ACF-2.5 samples was activated for 2.5 hours. Once the optimum activation time was obtained, the resulting capacitance did not increase but rather decreased as shown in the ACF-3.0 sample. The results of the specific capacitance in the ACF-2.5 might be used as a reference to conclude the activation time of 2.5 hours is the best in producing a supercapacitor carbon electrode from areca catechu husk. This specific capacitance is similar to the other studies as shown in Table 6. The energy density and power density can be calculated based on specific capacitance using a standard formula [26]. The highest energy density and power density obtained in this study were 5.73 Wh Kg^{-1} and 41.33 W Kg^{-1}, respectively.

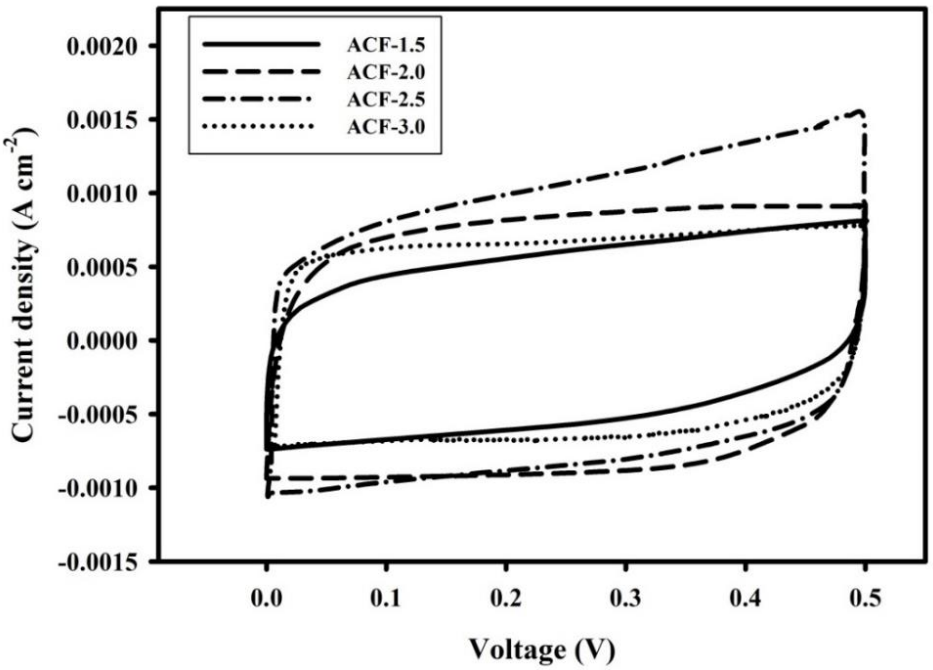

Figure 6. The cyclic voltammogram for ACF-1.5, ACF-2.0, ACF-2.5 and ACF-3.0 samples

Table 5. The (I_c) and (I_d) data, the average mass of electrode (m), and specific capacitance of supercapacitors (C_{sp}) for all samples

Sample codes	I_c (A)	I_d (A)	m (g)	C_{sp} (F g^{-1})
ACF-1.5	0.000679	-0.000789	0.01470	100
ACF-2.0	0.001026	-0.000974	0.01385	144
ACF-2.5	0.000939	-0.000850	0.01084	165
ACF-3.0	0.000546	-0.001001	0.01230	126

Table 6. Summary of various biomass-derived carbon materials for supercapacitor as well as their specific surface area and capacitance.

Biomass resources	S_{BET} ($m^2\ g^{-1}$)	C_{sp} ($F\ g^{-1}$)	References
Banana stem	835.939	170	[17]
Pineapple crown	684.035	150	[19]
Firwoods	1016	105	[27]
Cherry stone	1100-1300	230	[28]
Waste paper	416	160	[29]
Fungi	80.08	196	[30]
Fungus	1103	360	[31]
Rice husk	2804	278	[32]
Areca catechu	757.449	165	Present study

4. CONCLUSION

This study successfully demonstrated the synthesis of bridging carbon particles with carbon nanotubes as electrode supercapacitors. Generally, activated carbon electrodes are prepared from the areca catechu husk through chemical and physical activations. The KOH activator agents were chosen as chemical activation materials and physical activation time variations were the main focus of the study. Additionally, the carbonization and physical activation processes are carried out in one stage. The supercapacitor electrode delivered a specific capacitance of 165.04 F g^{-1} with a surface morphology showing hollow fiber nanotube. Furthermore, the hollow fiber structures such as nanotubes are among the structures which must be considered in improving the performance of capacitor electrodes. The use of areca catechu husk waste as a carbon electrodes material has great potential in high-performance energy storage systems.

ACKNOWLEDGEMENTS
The author would like to thank the DRPM Kemenristek-Dikti through the first year Project of PD with the title “high-density micro-and nano carbon fiber made from biomass based materials for supercapacitor electrodes” with contract number: 729/UN.19.5.1.3/PT.01.03/2019.

References

1. M.C.D. Santos, O. Kesler, A.L.M. Reddy, *J. Nanomaterials*, 1 (2012) 2012.
2. H. Luo, M. Wei, K. Wei, *J. Nanomaterials*, 1 (2009) 2009.
3. H. Liu, Y. Xu, C. Zhou, S. Geng, C. Wei, C. Yu, *J. Polymeric Mater. Pol. Biomaterials,* 66 (2017) 15.
4. V.B. Rekha, K. Ramachandralu, S. Vishak, *Int. J. Pharm Teach Res.,* 8 (2015) 521.
5. T.V. Ramachancra, G. Kamakshi, B.V. Shruti, *Renewable and Sustainable Energy Reviews*, 8 (2004) 1.
6. Badan Pusat Statistik (BPS). 2015. Produksi Tanaman Palma. Indonesia.
7. R. Barlina, *Buletin Palma*, 33 (2007) 96.

8. M. Natalia, Y.N. Sudhakar, M. Selvakumar, *Indian J. Chem. Technol.*, 20 (2013) 392.
9. E. Taer, Apriwandi, Yusriwandi, W. S. Mustika, Zulkifli, R. Taslim, Sugianto, B. Kurniasih, Agustino, P. Dewi, *AIP Conf. Proc.*, 1927 (2018) 030036-1.
10. E. Taer, A. Apriwandi, R. Taslim, U. Malik, Z. Usman, *Int. J. Electrochem. Sci.,* 14 (2019) 1318.
11. E. Taer, R. Taslim, Z. Aini, S.D. Hartati, and W.S. Mustika, *AIP Conf. Proc.,* 1801 (2017) 040004.
12. E. Taer, P. Dewi, Sugianto, R. Syech, R. Taslim, Salomo, Y. Susanti, A. Purnama, Apriwandi, Agustino, R.N. Setiadi, *AIP Conf. Proc.,* 1927 (2018) 030026-1.
13. A.G. Pandolfo, A.F. Hollenkamp, *J. Power Sources,* 157 (2006) 11.
14. E. Taer, A. Afrianda, Apriwandi, R. Taslim, A. Agustino, Awitdrus, R. Farma, *Int. J. Electrochem. Sci.,* 13 (2018) 10688.
15. L. Giraldo, J.C. Moreno-pirajan, *E-J. Chem.,* 9 (2012) 938.
16. J. Mi, X-r. Wang, R-j. Fan, W-h. Qu,W-c. Li, *Energy Fuels*, 26 (2012) 5321.
17. E. Taer, R. Taslim, W.S. Mustika, B. Kurniasih, Agustino, A. Afrianda, Apriwandi, *Int. J. Electrochem. Sci.,* 13 (2018) 8428.
18. E. Taer, A. Afrianda, R. Taslim, Krisman, Minarni, A. Agustino, A. Apriwandi, U. Malik, *J. Phys.: Conf. Ser.,* 1120 (2018) 012007.
19. E. Taer, A. Apriwandi, Y. S. Ningsih, R. Taslim, Agustino, *Int. J. Electrochem. Sci.,* 14 (2019) 2462.
20. Y.Z. Zhang, Z.J. Xing, Z.K. Duan, M. Li, Y. Wang, *Appl. Surface Sci.,* 315 (2014) 279.
21. K.Y. Foo, B.H. Hameed, *Bioresource Technol.,* 112 (2012) 143.
22. M. Deraman, R. Omar, S. Zakaria, I.R. Mustapa, M. Talib, *J. Mater. Sci.,* 37 (2002) 3329.
23. M. Deraman, R. Daik, S. Soltaninejad, N.S.M. Nor, Awitdrus, R. Farma, N.F. Mamat, N.H. Basri, M.A.R. Othman, *Adv Mater. Res.,* 1108 (2015) 1.
24. W.S.K. Sing, H.D. Everett, W.A.R. Haul, L. Moscou, A.R. Pierotti, J. Rouquerol, T. Siemieniewska, *Pure & App. Chem.,* 57 (1985) 603.
25. H. Chen, Y-c. Guo, F. Wang, G. Wang, P-r. Qi, X-h. Guo, F. Yu, B. Dai, *New Carbon Mater.,* 32 (2017) 592.
26. X. Ma, C. Ding, D. Li, M. Wu, Y. Yu, *Cellulose,* 25 (2018) 4743.
27. F.C. Wu, R.L. Tseng, C.C. Hu, *J. Power Sourc.,* 144 (2005) 302.
28. M. Olivares-Marin, J. A. Fernandez, M. J. Lazaro, *Mater. Chem. Phys.,* 114 (2009) 323.
29. D. Kalpana, S.H. Cho, S.B. Lee, *J. Power Sourc.,* 190 (2009) 587.
30. H. Zhu, X. Wang, F. Yang, *Adv. Mater.,*23 (2013) 2745.
31. C. Long, X. Chen, L. Jiang, *Nano Energy,* 12 (2015) 141–151.
32. D. Liu, W. Zhang, W. Huang, *Chinese Chem. Letters,* 30 (2019) 1315.